Calorimetric Measurements of the Total Hemispherical Emittance of Selective Surfaces at High Temperatures

A. Brunotte, M. Lazarov and R. Sizmann

Sektion Physik, Ludwig-Maximilians-Universität München,
Amalienstrasse 54, D-8000 München 40, Federal Republic of Germany

Abstract: An apparatus is presented for measuring the hemispherical emittance ε in a temperature range of 100 - 400 °C. It is designed especially for samples with low values of ε between 0.015 and 0.15. The error margin lies around 6% of the measured value. A polished stainless steel sample (PTB, Braunschweig, Germany) serves as reference reproducing the PTB-results within 2%. Measurements of solar selective absorbers, a TiN_xO_y-Cu tandem absorber, a multilayer cermet absorber and a Al_2O_3-Ni-Al absorber have been carried out. The values of ε range between 0.02 and 0.15 for 100 °C and between 0.035 and 0.3 for 400 °C. TiN_xO_y-Cu achieves the lowest values in both cases. The effects of temperature on the optical constants in the near IR of TiN_xO_y-Cu tandem layers are discussed. The results of measurements indicate a shift from dielectric to metallic behaviour with rising temperature.

1 Introduction

The performance of solar selective absorbers is characterized by the solar absorptance α, the hemispherical emittance ε and internal heat losses. Since thermal radiative losses of such absorbers increase proportionally to at least the fourth power of the temperature, low ε is the key for high temperature usage. A precise measurement of low values of ε (< 0.05) is an essential step in the development of suitable materials.

ε is frequently measured by determining the reflectance R at room temperature and calculating $\varepsilon = 1 - R$. However, this often yields unreliable results, as small errors in R produce large errors in small values of ε. Additionally, R is only measured for an incidence angle near normal and the angular distribution is not considered. Furthermore, the temperature dependence of optical material constants has to be taken into account.

On the other hand, the calorimetric method presented in this paper can yield highly accurate results of ε. These are obtained under conditions comparable to those in solar vacuum collectors. The calorimetric method uses heat fluxes from and to the sample, which is kept at constant temperature T_s. In thermal equilibrium $\varepsilon(T_s)$ can be calculated by

$$\varepsilon(T_s) = \frac{P_h - P_u}{\sigma \cdot T_s^4 \cdot A_s} , \quad (1)$$

where P_h is the electrical heating power, P_u the sum of all other heat fluxes, σ the Stefan-Boltzmann constant and A_s the emitting area of the sample.

0-8194-0900-6/92/$4.00

In order to minimize P_u, R.Sadler, L.Hemmerdinger and I.Rando [1] surrounded the back and lateral faces of the sample with a guard heater adjusted to T_s. This inevitably produced a gap. They covered it with a thin mylar foil touching the rim of the sample. H.Willrath and G.B.Smith [2] simply left the gap uncovered. In both cases, the influence of the gap remained unknown quantity. W.W.Beens, M.Sikkens and J.L.Verster [3] fixed a solid lid onto the guard heater leaving a circular opening for the sample. They then measured the heating power in dependence on the distance d between the sample and the opening. They extrapolated to $d = 0$ but made no statement about P_u at this point.

In this work the greatest part of P_u is *measured* and the remainder is calculated. The accuracy of the method is demonstrated and then applied to spectral selective TiN_xO_y-Cu absorbers. The influence of temperature on the optical constants of those absorbers is evaluated and explained using a simple model.

2 Description of the Emissometer

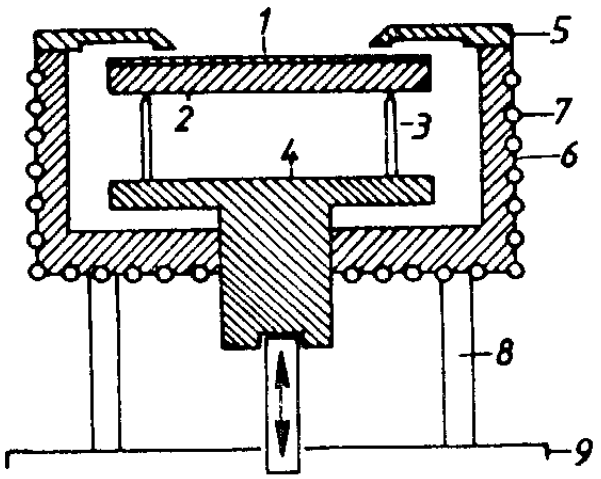

Figure 1: Cross section of the emissometer.
1: sample; 2: support; 3: poles of glass ceramics; 4: table; 5: cover; 6: guard heater block; 7: heating; 8: poles of the block of ceramics; 9: ground.

Figure 1 shows a cross section of the emissometer. It is fixed in a vacuum chamber ($p < 10^{-5}$ Pa) with blackened walls cooled with liquid nitrogen. A sample (1) is placed on the support (2). Both are partly surrounded by a copper guard heater (6). The cover (5) closes the guard heater almost completely. A circular opening (r =3 cm) is left. Three thin poles (3) of glass ceramics carry the support. These poles stand on a stainless steel table (4), which can be moved up and down from the outside of the vacuum chamber. In that manner the distance between sample and cover can be varied to measure and to correct the influence of the gap between sample and cover.

Radiation exchange and heat conduction through cables and poles result in heat fluxes between sample and guard heater. However, if isothermal conditions are reached, the heat flux is always zero. Temperature differences ΔT are measured by four thermocouples, one of each placed in (2),(4),(5) and (6). The ΔT measured can be adjusted to be smaller than 0.03 ± 0.01 K during experiment. All four parts can be heated separately and are usually adjusted to the same temperature (100 °C $\leq T \leq$ 400 °C).

3 Accuracy of the Emissometer

The base heat flux: An alternative for the open cover can be an cover entirely shut. This allows an estimation of the sum of all heat fluxes from and to the sample with closed cover, P_{base}, *excluding* the emitted radiant flux of the sample. If the measured $\Delta T = 0$, one might expect P_{base} to be zero, too. This proved wrong in experiment. Two factors may account for this:

1. The sample looses heat to the surroundings of the vacuum chamber through cables. (P_{sa})
2. The temperature distribution of the guard heater is not homogeneous. Therefore the temperature of the thermocouples and other places of the guard heater may differ. The sample can loose or gain heat even when the measured temperature differences ΔT are zero. (P_{sg})

$$P_{base}\,|_{\Delta T=0} \quad = \quad P_{sa}(\Delta T_{sa}) \quad + \quad P_{sg}(T_s), \tag{2}$$

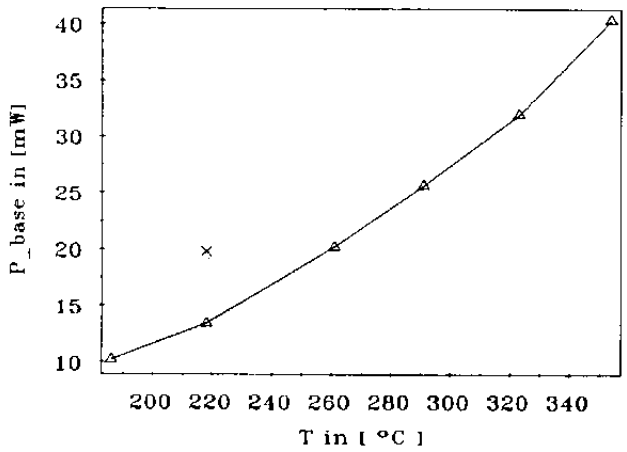

Figure 2: Temperature dependence of the measured heating power with completely closed cover (P_{base}). The line represents a TiN_xO_y-Cu sample. The cross marks a measurement point from a stainless steel sample with an emittance three times higher.

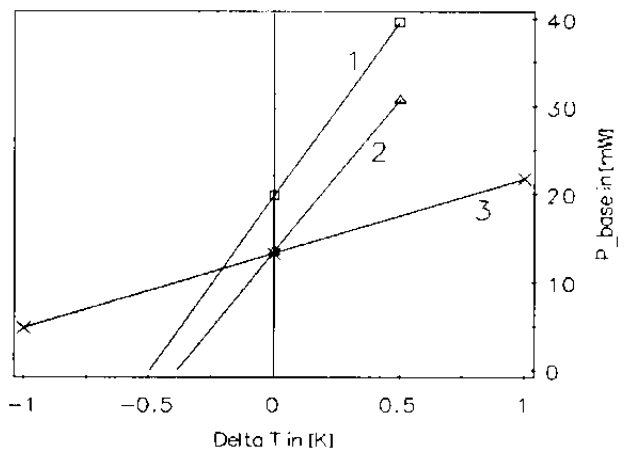

Figure 3: Effect of cover and guard heater on P_{base}. Line 1: P_{base} in dependence on the temperature difference ΔT_{sg} between sample and guard of a steel sample. Line 2: P_{base} in dependence on the temperature difference ΔT_{sg} between sample and guard of a TiN_xO_y-Cu sample. Line 3: P_{base} in dependence on the temperature difference ΔT_{sc} between sample and cover of a TiN_xO_y-Cu sample.

In Figure 2 the dependence of P_{base} on the temperature T_s is shown. The curve represents a TiN_xO_y-Cu tandem sample. The temperature dependence is not linear. Evidently, radiation exchange is a main cause for the measured values P_{base}. The emittance of the TiN_xO_y-Cu sample is about one third of the emittance of a polished stainless steel sample (see paragraph "Reference sample"). P_{base}

$P_{base}(\mathrm{TiN_xO_y})$	$P_{base}(\mathrm{steel})$	$\varepsilon_{\mathrm{TiN_xO_y}}$	$\varepsilon_{\mathrm{steel}}$	$\tilde{R}_{sc}(\mathrm{TiN_xO_y})$	P_{base}^{block}	$P_{base}^{cover}(\mathrm{TiN_xO_y})$	ΔT_{sc}^{eff}
13.5 mW	19.8 mW	0.050	0.156	8.5 mW/K	10.4 mW	3.1 mW	0.36 K

Table 1: Contribution of cover in P_{base} for TiN_xO_y. P_{base}^{block} is calculated using equation 5 and ΔT_{sc}^{eff} is calculated using equation 3.

of the steel sample is significantly higher (cross), a proof that P_{base} depends on the emittance of any sample and thus $P_{sg}(T_s)$ is not zero. In no experiment did the distance between sample and cover exceed 0.15 mm. Therefore, the sample exchanges heat mainly with the cover, and there must be an effective temperature difference between sample and cover $\Delta T_{sc}^{eff} > 0$ even when the *measured* ΔT_{sc} is zero.

In Figure 3 the effect of the cover on P_{base} is demonstrated. The temperature differences ΔT_{sg} between both samples and the guard and ΔT_{sc} between the TiN_xO_y-Cu sample and the cover have been varied. The gradients $\tilde{R}$ of the straight lines give information about the thermal coupling to the sample:

$$\tilde{R}_i = \frac{\Delta P}{\Delta T_i} \tag{3}$$

$\tilde{R}_{sc}(\mathrm{TiN_xO_y})$ (Line 3) is about one third of $\tilde{R}_{sg}(\mathrm{TiN_xO_y})$ (Line 2). The gradient $\tilde{R}_{sg}(\mathrm{steel})$ (Line 1) is greater than $\tilde{R}_{sg}(\mathrm{TiN_xO_y})$.

Because of the narrow distance between sample and cover (d < 0.5 mm), it is assumed that *only* the radiation exchange of sample and cover is dependent on the emittance of the sample.

In order to estimate the part of P_{base}, which is independent on the emittance of the sample, the following calculation has been carried out:

$$P_{base}|_{\Delta T_{sg}=0} = P_{base}^{cover} + P_{base}^{block} \tag{4}$$

$$\frac{P_{base}^{cover}(\mathrm{TiN_xO_y})}{P_{base}^{cover}(\mathrm{steel})} = \frac{\varepsilon_{\mathrm{TiN_xO_y}}}{\varepsilon_{\mathrm{steel}}} \quad ,$$

where, $P_{sa}(\Delta T_{sa})$ (equation 2) is a part of P_{base}^{cover}. Then, the effective temperature difference between sample and cover ΔT_{sc}^{eff} can be calculated from the gradient $\tilde{R}_{sc}(\mathrm{TiN_xO_y})$ (see Figure 3 and equation 3). The values for 218 °C are listed in Table 1. For the TiN_xO_y-Cu sample the heat transfer between support and guard heater block dominates over the heat transfer between sample and cover. ΔT_{sc}^{eff} is small. The value can be explained with heat conduction through the cover and the position of the thermocouple placed in the cover.

For correction of the measured heat fluxes P_h we use (see equation 1):

$$P_u := \left(P_{base}^{block} + \frac{P_{base}^{cover}}{2}\right) \pm \frac{P_{base}^{cover}}{2} \tag{5}$$

$P_{base}^{cover}/2$ is the uncertainty in P_u, because measurements with closed cover provide no information which parts of the cover and the sample exchange heat with each other by emitting and absorbing radiation. [1]

Influence of the gap between cover and sample: Figure 4 shows results of the heating power in relation to the gap width d. d is derived from the capacity of a ring shaped capacitor with one sheet electrically insulated in the cover and the other placed on the support. The emittance of the TiN_xO_y-Cu sample at 376 °C is about 0.03. The fit curve, a polynom of third order, is similar to that in [3]. We tried, according to Beens et al. ([3]), to model the behaviour, but without knowledge about the angular dependence of the optical constants, we failed. However, it is only necessary to know the extrapolated value of P_h at $d = 0$.

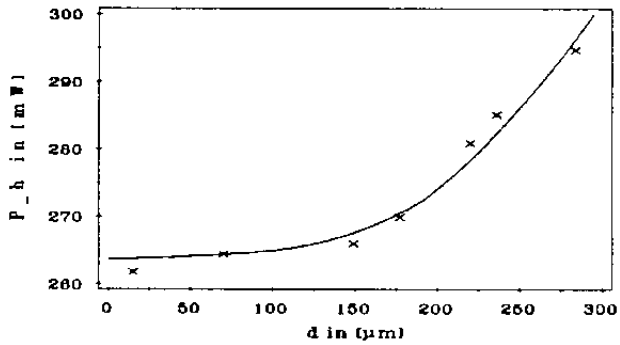

Figure 4: Measured heating power P_h in dependence of the gap width d between sample and cover.

Influence of cover at gap width zero: There is still an influence of the cover on the measured value of P_h at $d = 0$: The edge of the opening in the cover emits radiation in the direction of the sample and the sample absorbes a part of it.

A computer simulation considering the angular dependence of α_s and ε_c (≈ 0.1) has been carried out. The radiant flux, which is emitted by the cover and absorbed by the sample, P_{cs} has been integrated. The relative error f is given by

$$f|_{d=0} = \frac{P_{cs}}{\varepsilon(T_s) \cdot \sigma \cdot T_s^4 \cdot A_s} \tag{6}$$

Assuming the same angular distribution of the sample's absorptance and the cover's emittance at any temperature, f appears not to be temperature dependent. Compared with the effect of P_{base}, f is of the same order of magnitude (Table 3).

Error analysis: Considering equation 1 the error of the determined emittance $\varepsilon(T_s)$ can be estimated. In Table 2 the effects of the various error terms are listed. The values in the column "relative to $\varepsilon(T_s)$" are solely measurement errors. The calculation of the absolute error as a result of P_u has been explained above, but not the "heat capacitance term". The temperatures at any

[1] With an open cover the cover may gain the same heat flux from the sample or may not gain anything.

	Symbol	relative to $\varepsilon(T_s)$	absolute
Absolute temperature	T	4 K / T_s	-
Area of the sample	A_s	< 0.001	-
Heating power	P_h	0.01	-
Heat capacitance term	$C_s \cdot \frac{dT}{dt}$	-	individual
Unwanted heat fluxes	P_u	-	P_{base}^{cover} / $(2 \cdot \sigma \cdot T_s'^4 \cdot A_s)$
Rad. flux cover-sample	P_{cs}	≈ 0.02	-

Table 2: Absolute and relative errors of measured emittance. Relative means fraction of the measured emittance; absolute means additional (±) to the emittance.

measurement are adjusted to one constant value. Small temporal changes have been taken into account by the heat capacitance term. The value $5 \cdot 10^{-5}$, listed in Table 3, is typical.

The vacuum chamber is cooled with liquid nitrogen and the radiation flux emitted from the blackened walls can be neglected.

For the TiN_xO_y-Cu sample mentioned above the errors are calculated and listed in Table 3. P_u and P_{cs} are systematic errors. When results of the emissometer are compared, the much smaller statistical errors have to be considered.

Reference sample: A polished stainless steel reference sample is measured in the emissometer and in a device of the Physikalisch Technische Bundesanstalt (PTB), Braunschweig, Germany, at the same temperature [4], [5]. The PTB measured the angular dependent emittance $\varepsilon(\theta)$ at five different polar angles ($0° \leq \theta \leq 75°$) and calculated the hemispherical emittance: $\varepsilon_{steel}(218\,°C) = 0.154$. The result obtained of the presented emissometer is: $\varepsilon_{steel}(218\,°C) = 0.156$.

4 Measurements on Different Solar Selective Absorbers

Besides the reference sample the emittance of a polished molybdenum sample and two different selective absorbers were measured (Figure 5). Molybdenum is often proposed as IR-reflector for high temperature selective absorbers [6]. The emittance is above 0.04 (lowest curve in Figure 5). A coating on molybdenum, deposited to increase the solar absorptance, in general increased the emittance. Therefore, this material is not considered to be suitable for high temperature applications ($T > 200\,°C$) without concentration.

The other two lines in Figure 5 represent a multilayer cermet absorber, developed by the Institut Für Solare Energiesysteme (ISE) Freiburg, Germany [7] (middle curve) and an Al_2O_3-Ni-Al absorber from the company Thermosolar in Regensburg, Germany (upper curves). The cermet coating shows

Symbol	relative to $\varepsilon(T_s)$ in %	absolute
T	0.8	0.0004
A_s	0.1	0.00005
P_h	1	0.0005
$C_s \cdot \frac{dT}{dt}$	0.1	0.00005
P_u	2.2	0.0011
P_{cs}	2.0	0.001
$\sum$	6.2	0.0031

Table 3: Error listing of a TiN_xO_y-Cu sample at 218 °C. The result of the measurement is: $\varepsilon_{TiN_xO_y} = 0.050 \pm 0.003$. Comparing results of the emissometer among themselves the error is lower.

a high absorptance of 0.94 [7] and an emittance below 0.15. A slight degradation of this coating is observed above 250 °C, which confirms the results of aging tests performed by Graf et al. [7]. This coating is suitable for applications with temperatures up to 150 °C. The Al_2O_3-Ni-Al coating also has an absorptance above 0.92, and the emittance shifted during the measurement to lower values. No shift in the absorptance could be detected after the calorimetric measurements. This indicates a potential for optimization of this material.

5 TiN_xO_y-Cu Absorbers

Measurements and sample characterisation: We measured a series of low emitting TiN_xO_y-Cu selective absorbers. The emittance of these coatings varies between 0.03 and 0.05 at 200°C depending on preparation conditions, substrate roughness and thickness of the films. To produce these absorbers, copper was evaporated on polished copper substrates. The TiN_xO_yfilm was deposited by activated reactive evaporation ARE [8]. All coatings were prepared under similar conditions without breaking vacuum. The intention was, to vary only the thickness of the TiN_xO_yfilm. Titanium was evaporated with a rate of 0.2nm/s in a reactive atmosphere of nitrogen and oxygen. The partial pressures of nitrogen and oxygen were 10^{-3}hPa and 10^{-4}hPa, respectively. The substrate temperature during evaporation was kept at 170 °C. Further details on sample preparation are given elsewhere [9]. The applied nitrogen to oxygen pressure ratio of approximately 10 provides for highly selective properties for solar applications.

The emittance as a function of temperature for three films with different thicknesses is shown in Figure 6. Further properties of the investigated films are summarized in Table 4, including the calculated thermal efficiency η at $T = 250$°C and an solar irradiance E of 1000 W/m^2 according to the equation:

$$\eta = \alpha - \varepsilon(T) \cdot \sigma \cdot (T^4 - T_a^4)/E. \tag{7}$$

As ambient temperature T_a we used 293 K.

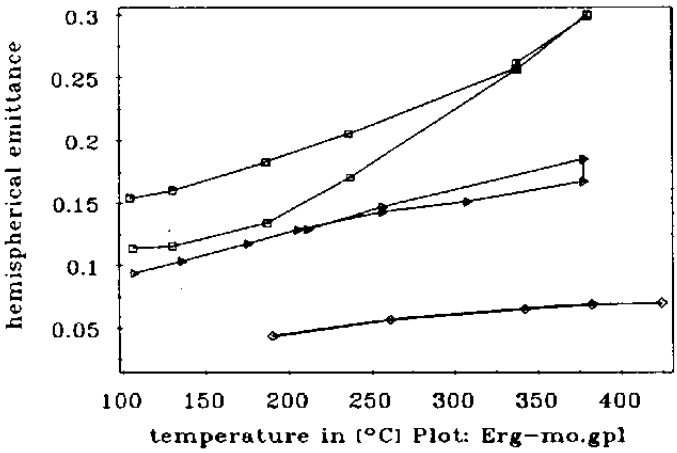

Figure 5: Hemispherical emittance versus temperature of polished molybdenum (lowest curve), a cermet multilayer (middle curve) and Al_2O_3-Ni-Al absorber (upper two curves). Both absorbers shifted their properties during measurements.

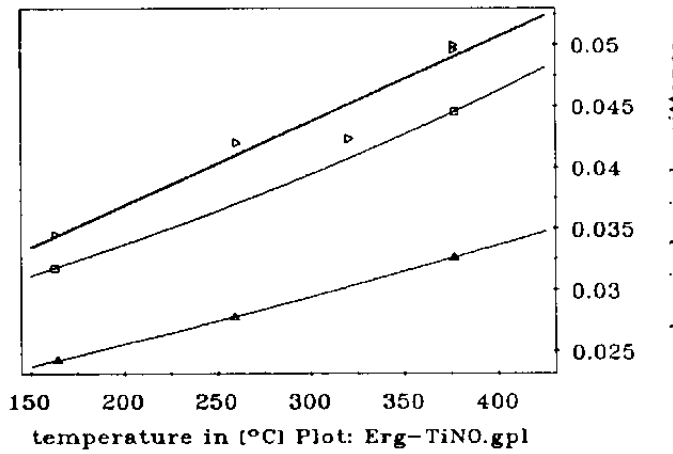

Figure 6: Hemispherical emittance versus temperature of TiN_xO_y-Cu absorbes with different thicknesses, but same preparation conditions. The lowest curve refferes to sample #160, the curves above to #163 and #165 respectively. For details of sample characterization see Table 4.

With increasing thickness and roughness both, the absorptance and the emittance increase.

Discussion: The accuracy of the presented calorimetric measurements allows to examine the effects of substrate roughness and temperature on low emitting solar absorbers.

A theoretical value for the hemispherical emittance can be derived from the optical constants and the roughness δ of the interfaces. The optical constants of the involved materials $\tilde{n}_{TiN_xO_y}$ (see Figure 7) and $\tilde{n}_{Cu}$ were derived from measurements at room temperature. The approach and the used formulas is printed in the Appendix. We calculated the theoretical hemispherical emittance as a function of thickness at 300 °C for the highest and lowest roughness δ of the samples. These results are shown in the lower two curves in Figure 8. They are compared to the experimental values (points).

Clearly, the emittance of the thick coatings differs substantially from calculations, where only room temperature data were involved. The difference can be assigned to the shift of the optical constants $\tilde{n}_{TiN_xO_y}(T,\lambda)$ and $\tilde{n}_{Cu}(T,\lambda)$ with temperature. A correction of $\tilde{n}_{Cu}$ applying a Drude model [10] shifts the ε curve to a higher level but does not explain the large increase of the emittance for the thicker coatings. The TiN_xO_yfilm itself consist of a mixture of dielectric (TiO_2) and metallic (TiN and TiO) phases, as demonstrated by XPS and UPS measurements [11]. The behaviour in the near infrared is not metallic at room temperature, as seen from the optical constants in Figure 7. At room temperature the dielectric behaviour dominates this wavelength region.

sample	thickness [nm]	emittance	absorptance	roughness [nm]	efficiency
160	28	0.027	0.63	20	0.53
161	36	0.024	0.65	20	0.56
162	44	0.029	0.74	20	0.63
163	47	0.036	0.80	26	0.67
164	53	0.032	0.75	10	0.63
165	59	0.040	0.84	31	0.69
166	58	0.039	0.85	35	0.70
167	68	0.040	0.82	34	0.67
168	72	0.048	0.89	56	0.71

Table 4: Sample characterization. Summary of the properties of the investigated samples: thickness as measured by X-Ray diffraction at grazing incidence angles (GXR), emittance measured at 250 °C, absorptance and roughness δ, determined as explained in the Appendix. The thermal efficiency was calculated according to equation 7 with 1000 W/m^2 insolation.

To evaluate a shift in the optical constants with temperature we used a crude model. The optical constants of the film $\tilde{n}_{TiN_xO_y}$ and the substrate $\tilde{n}_{Cu}$ at room temperature T_R were corrected by an additive temperature but not wavelength dependent complex number:

$$\begin{aligned} \tilde{n}_{TiN_xO_y}(T,\lambda) &:= \tilde{n}_{TiN_xO_y}(T_R,\lambda) + \tilde{C}_{TiN_xO_y}(T) \\ &\text{and} \\ \tilde{n}_{Cu}(T,\lambda) &:= \tilde{n}_{Cu}(T_R,\lambda) + \tilde{C}_{Cu}(T). \end{aligned} \tag{8}$$

The four constants, the real- and imaginary parts of $\tilde{C}_{TiN_xO_y}$ and $\tilde{C}_{Cu}$ respectively, were determined by a numerical fit [12] of the experimental data for each temperature. The upper curves in Figure 8 demonstrate, that reasonable fits are achieved with this approach. The results are summarized in Table 5. The accuracy was determinad by parabolic approximation of the topology around the fitting results.

	150°C	200°C	250°C	300°C	350°C	400°C	accuracy
$\Re(\tilde{C}_{TiN_xO_y})$	0.1	0.1	0.22	0.29	0.35	0.35	$\pm$0.1
$\Im(\tilde{C}_{TiN_xO_y})$	0.40	0.80	0.9	0.9	1.0	1.10	$\pm$0.08
$\Re(\tilde{C}_{Cu})$	-0.08	-0.06	-0.07	-0.05	-0.04	-0.09	$\pm$0.1
$\Im(\tilde{C}_{Cu})$	-0.20	-0.18	-0.25	-0.22	-0.32	-0.28	$\pm$0.1

Table 5: Temperature correction of the optical constants. Real and imaginary part of the correction numbers for different temperatures.

The most pronounced effect results from the imaginary part of $\tilde{C}_{TiN_xO_y}$. This fit-parameter was determined with the best accuracy. Increasing IR-absorption in the film, which is equivalent to

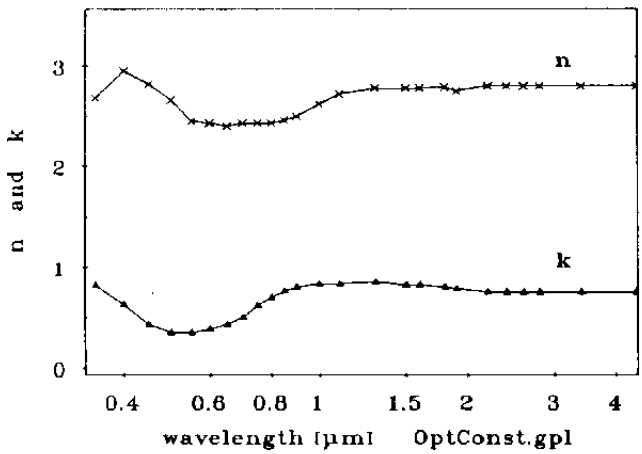

Figure 7: Optical constants of the TiN_xO_yfilms. Real part – upper cuve; imaginary part – lower curve. The error varies with wavelength between 0.05 and 0.2.

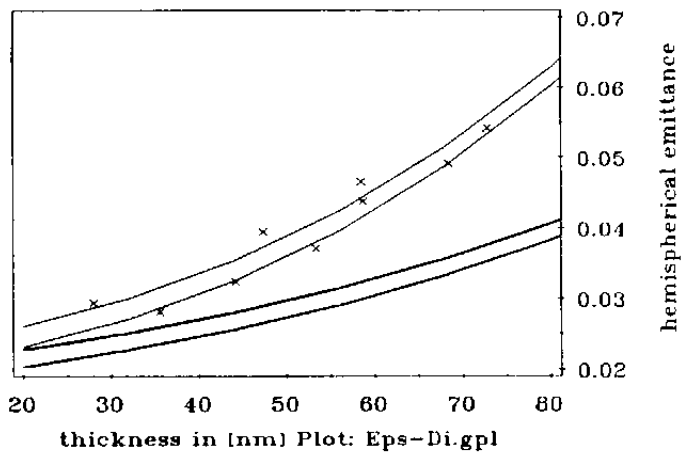

Figure 8: Hemispherical emittance versus thickness of the TiN_xO_ylayer at 300°C. Measurements and theoretical curves (see text).

increasing $\Im(\tilde{C}_{TiN_xO_y})$, closes the gap between theoretical and measured values at small film thicknesses. The real part $\Re(\tilde{C}_{TiN_xO_y})$ has the effect of increasing the slope of the curve for high thicknesses, but a minor effect on the emittance of thinner films. The shift in the optical properties of copper can hardly be determined beyond the error limits. The calculated value of $\tilde{C}_{Cu}$ is $\tilde{n}_{Cu}/40$ with a high uncertainty. The effect of $\tilde{C}_{Cu}$ is a shift to a higher emittance, independent on the film thickness.

The simple model suggests that the average optical constants $\tilde{n}_{TiN_xO_y}$ of the TiN_xO_yfilm increase in the infrared region with temperature. This can be explained when the coating shifts from dielectric to metallic behaviour. For example, the optical constant of TiN at 5 μm is $15 - 34i$ [13]. This effect is reversible, since no change in properties can be observed after the calorimetric measurements or when the measurements are repeated.

The observed facts can be explained by the following preliminary considerations on the structure of the coatings and diffusion of oxygen. From investigation of the chemical composition of the coatings by XPS and UPS measurements [11] the film structure can be derived. They consist of a columnar grown mixture of TiN and TiO, both metallic materials with a pronounced Fermi edge, as observed in UPS. This structure is covered by a thin TiO_2 layer and amorphous titanium-oxides can be found in-between the columns. Both, the TiO_2 layer and the intermedial oxides form immediately after exposure to air [9]. This aging process can be partly reversed when heating the samples in vacuum [11]. The oxygen spoils the metallic behaviour natural for TiN and TiO and produces the low emittance of the TiN_xO_y-Cu absorbers. When the samples are heated to higher temperatures the oxygen partly escapes so that the coatings become more metallic and the emittance increases.

Further investigation is needed to confirm this picture.

Acknowledgements: The assistance of H. Klank during measurements and Dr. J. Lohrengel for supplying the reference sample is acknowledged. This work was supported by the Bundesminisiterium für Forschung und Technologie, Bonn, Germany.

A Appendix

A detailed description of the following can be found in [14].

The emittance of TiN_xO_y-Cu absorbers can be calculated from the spectral, directional-hemispherical reflectance R_{sum} derived from the optical constants of the involved materials ($\tilde{n}_{TiN_xO_y}$ and $\tilde{n}_{Cu}$) and the roughness δ of the interfaces:[2]

$$\varepsilon_{hem} := \frac{2\pi}{\sigma \cdot T^4} \cdot \int_0^\infty \mathrm{d}\lambda \, L_\lambda(\lambda, T) \int_0^{\frac{\pi}{2}} \mathrm{d}\vartheta \, \cos\vartheta \sin\vartheta \, [1 - R_{sum}(\lambda, \vartheta)] \quad , \tag{9}$$

where $L_\lambda(\lambda, T)$ is the Planck distribution of the spectral density of a black body with the temperature T. R_{sum} is the sum of specular reflectance R_{coh} and diffuse reflectance.

Given $\tilde{n}_{TiN_xO_y}$ and $\tilde{n}_{Cu}$ the specular reflectance R_{coh} of the samples can be calculated using Airy summation and modified Fresnel coefficients (r_{mod}) according to a model introduced by Vidal et al. [15] which takes roughness of interfaces into account. Equation 10 gives the fresnel coefficients of a rough interface between two media with the optical constants $\tilde{n}_1$ and $\tilde{n}_2$, as long as the mean square of the height distribution δ is small compared to the wavelength.[3]

$$r_{mod}(\vartheta) = r \cdot \exp\left\{-2\Re(\tilde{n}_1 \cos\tilde{\vartheta}_1) \cdot \Re(\tilde{n}_2 \cos\tilde{\vartheta}_2) \cdot \left(\frac{2\pi\delta}{\lambda}\right)^2\right\}. \tag{10}$$

To calculate R_{sum} employing equation 11 the diffuse reflectance is needed. We applied the approach by Elson et al. [16] which takes the correlation length of the height distribution of a rough surface into account:

$$R_{sum}(\vartheta) = R_{coh} + \frac{4}{3}(R_{\delta=0}(\vartheta) - R_{coh}(\vartheta)) \cdot \left(\frac{\pi\sigma_c}{\lambda}\right)^2 \tag{11}$$

The optical constants of the TiN_xO_ylayer were determined from room temperature reflectance and transmittance measurements on films deposited on glass substrates under the same deposition conditions as used for the investigated samples. The inversion of the Fresnel formulas was performed by a graphical method [17]. The results for the discussed coatings are presented in Figure 7. For numerical calculations $\tilde{n}_{TiN_xO_y}(\lambda)$ was assumed to be constant beyond $4\mu m$ and was assigned the value $\tilde{n}_{TiN_xO_y}(\lambda = 4.0\mu m)$. $\tilde{n}_{Cu}$ was taken from literature [18]. The root mean square roughness δ and the correlation length σ_c were determined from a fit of the theoretical curve to the reflectance data according to equation 11.

Literature

[1] L.Hemmerdinger R.Sadler and I.Rando. Emissometer, a device for measuring total hemispherical emittance. *NASA SP 29-31, NASA*, p.217-223, 1963.

[2] Azimuthal isotropy is assumed here.

[3] According to Vidal [15], both polarisation states have to be modified by the same factor.

[2] H.Willrath and G.B.Smith. A New Transient Temperature Emissometer. *Solar Energy Materials*, 4:31–46, 1980.

[3] W.W.Beens M.Sikkens and J.L.Verster. An emissometer with high accuracy for determination of the total hemispherical emittance of surfaces. *Journal of Physics E: Scientific Instruments*, 13:873–876, 1980.

[4] M.Rasper J.Lohrengel. *Gesamtemissionsgrad von sandgestrahlten Oberflächen des Stahls 1.4301 und von mit rostfreiem Stahl beschichteten Glasoberflächen.* Band 99, PTB, Braunschweig und Berlin, Germany, 4/1989.

[5] J.Lohrengel. *Determination of the surface temperature of poor heat conducting materals by radiation measurements from 60 °Cto 250 °Cin vacuum.* Volume 21, Springer Verlag, Heidelberg und Berlin, Germany, 1987.

[6] B.O.Seraphin (Ed.). *Spectrally Selective Surface and Their Impact on Photothermal Solar Energy Conversion.* Volume 31, Springer, Berlin, 1979.

[7] W.Graf, M.Koehl, and V.Wittwer. Production and Characterization of Large-area Sputtered Selective Solar Absorber Coatings. In *Proceedings of Optical Materials Technology for Energy Efficiency and Solar Energy Conversion XI, 1992, Toulouse, France, to be presented*, 1992.

[8] Bunshah R.F. and Raguram A.C. Activated Reactive Evaporation Process for High Rate Deposition of Compounds. *J. Vac. Sci. Technol.*, **9**:1385–1388, 1972.

[9] M.Lazarov, B.Röhle, T.Eisenhammer, and R.Sizmann. TiN_xO_y-Cu Coatings for Low-Emissive Solar-Selective Absorbers. In *Proceedings of Optical Materials Technology for Energy Efficiency and Solar Energy Conversion X, Proc. SPIE 1536*, pages 183–193, 1991.

[10] R.Smalley and A.J.Sievers. The total hemispherical emissivity of copper. *J.Opt.Soc.Am.*, **68**:1516–1519, 1978.

[11] J.Eitle, P.Oelhafen, M.Lazarov, and R.Sizmann. Chemical Composition of TiN_xO_y-Cu Solar Selective Absorbers. In *Proceedings of Optical Materials Technology for Energy Efficiency and Solar Energy Conversion XI, 1992, Toulouse, France, to be presented*, 1992.

[12] W.Spirkl. Dynamic SDHW Testing Program Manual. Available from: DIN, Postfach 1107, D-1000 Berlin 30, FRG, 1.19 edition, 1992.

[13] Karlsson B., Shimshok R.P., Seraphin B.O., and J.C. Haygarth. Optical Properties of CVD-Coated *TiN*, *ZrN* and HfN. *Solar Energy Materials*, **7**:401–411, 1983.

[14] M.Lazarov, A.Brunotte, T.Eisenhammer, R.Sizmann, W.Graf, and V.Wittwer. Effects of Roughness on TiN_xO_y-Cu Selective Absorbers. In *Proceedings of Optical Materials Technology for Energy Efficiency and Solar Energy Conversion XI, 1992, Toulouse, France, to be presented*, 1992.

[15] Vidal B. and Vincent P. Metallic Multilayers for X Rays Using Classical Thin-Film Theory. *Applied Optics*, **23(11)**:1794–1801, 1984.

[16] Elson J.M., Rah J.P., and Bennett J.M. Relationship of the Total Integrated Scattering from Multilayer-Coated Optics to Angle of Incidence, Polarization, Correlation Length, and Roughness Cross-Correlation Properties. *Applied Optics*, **22(20)**:3207–3219, 1983.

[17] T.C.Paulick. Inversion of normal-incidence (R,T) measurements to obtain $n + ik$ for thin films. *Appl.Opt.*, **25**:562–564, 1986.

[18] M.A.Ordal, L.L.Long, R.J.Bell, S.E.Bell, R.R.Bell, Jr. R.W.Alexander, and C.A.Ward. Optical properties of metals Al, Co, Cu, Au, Fe, Pb, Ni, Pd, Pt, Ag, Ti, and W in the infrared and far infrared. *Appl.Opt.*, **22**:1099–1119, 1983.